Martinez Feliu, A.; Arribas Viana, MDLD.; Concepción Heydorn, P.; Moussa-Martí, S. (2013). New bifunctional Ni H-Beta catalysts for the heterogeneous oligomerization of ethylene. Applied Catalysis A General. 467:509-518. doi:10.1016/j.apcata.2013.08.021

New bifunctional Ni-H-Beta catalysts for the heterogeneous oligomerization of ethylene

Agustín Martínez*, Maria A. Arribas, P. Concepción, Sara Moussa

Instituto de Tecnología Química, CSIC-UPV, Avda. de los Naranjos s/n,

46022 Valencia, Spain

*Corresponding author. Phone: +34 963 877 808. Fax: +34 963 877 809. *E-mail address:* amart@itq.upv.es.

Abstract

The development of sustainable active and stable heterogeneous catalysts for the oligomerization of ethylene to replace the unfriendly homogenous systems based on transition metal complexes currently applied in the industry still remains a challenge. In this work we show that bifunctional catalysts comprised of Ni loaded on nanocrystalline zeolite H-Beta can efficiently catalyze the oligomerization of ethylene with high stability and selectivity to liquid oligomers under mild reaction conditions. Ni-Beta catalysts were prepared starting from a commercial nanocrystalline H-Beta sample with Si/Al ratio of 12 *via* both ionic exchange (1.0-2.5 wt% Ni) and incipient wetness impregnation (1.1-10.0 wt% Ni) using aqueous $Ni(NO_3)_2$ solutions, followed by air-calcination at 550ºC. The Ni-Beta catalysts exhibited no signs of deactivation under the studied conditions (T= 120ºC, P_{tot}= 3.5 MPa, P_{C2H4}= 2.6 MPa, WHSV= 2.1 h^{-1}, TOS= 0-9 h). The conversion of ethylene increased linearly with increasing Ni loading up to ca. 2.5 wt%, irrespective of the method of Ni incorporation. Then, the conversion leveled off and attained a value of ca. 87% at higher Ni loadings (impregnated series), concurring with the development of large, XRD-visible, NiO crystallites sizing ca. 7-16 nm. Interestingly, the disappearance of Brønsted acid sites upon Ni incorporation increased linearly up to Ni contents of ca. 2.5 wt% and then leveled off, thus paralleling the activity trend. This fact indirectly suggests that Ni^{2+} cations replacing H^+ in ion exchange positions could be the active sites responsible for the activity of Ni-Beta catalysts. Direct evidence for the nature of the active Ni sites was obtained from low temperature (-20ºC) CO adsorption and ethylene-CO co-adsorption experiments followed by FTIR. CO-FTIR results ruled out the participation of Ni^+ ions and provided support for the assignation of

ion exchanged Ni^{2+} species as the likely active sites in Ni-Beta catalysts. Additionally, most active Ni-Beta catalysts displayed a non-Schulz-Flory product distribution with high selectivity to liquid oligomers (≥ 60 wt%) and high degree of branching due to the contribution of the *hetero-oligomerization* pathway involving zeolite Brønsted acid sites.

Keywords: Bifunctional catalyst; Ni-Beta zeolite; ethylene oligomerization; low temperature CO-FTIR; active Ni sites.

1. INTRODUCTION

Linear α-olefins (LAOs) are valuable intermediates in the synthesis of a wide range of industrial and consumer products such as detergents, synthetic lubricants, surfactants, and plasticizer alcohols. Short-chain LAOs (C_4-C_6) are also used as co-monomers in the production of linear low-density polyethylene (LLDPE). LAOs are currently produced through the liquid-phase oligomerization of ethylene using homogeneous catalysts comprising a transition metal (e.g. Ni Co, Cr, Fe, etc.) complex assisted by an alkyl aluminum co-catalyst [1]. The homogeneous phase oligomerization processes suffer from several drawbacks, such as the high sensitivity of the organometallic catalyst to impurities in the feed, the cumbersome separation of the catalyst from the products and the solvent, and the limited catalyst reusability, among others. Supporting the organometallic complex on a high surface area porous solid, such as the ordered mesoporous MCM-41 silica [2], may be regarded as a partial solution to the issue though, in this case, the potential contamination of the product by metal leached to the liquid phase from the supported catalyst has to be considered. It is, thus, clear that the development of alternative true heterogeneous greener catalysts enabling the oligomerization of ethylene at mild conditions is highly desirable though challenging.

Contrarily to the oligomerization of propene and higher alkenes, the initial activation and oligomerization of ethylene can hardly proceed *via* acid catalysis which would involve highly instable primary carbocation intermediates. In this respect, bifunctional solid catalysts comprising *isolated* nickel ions (thus mimicking the structure of the active site in the homogeneous systems) in ion-exchangeable aluminosilicate matrices have been found active in the

oligomerization of ethylene at moderate temperatures [3,4,5,6,7,8,9,10,11]. In these catalysts, Ni cations in ion exchanged positions are presumed to be responsible for the activation of ethylene and its oligomerization into linear odd-numbered C_{4+} α-olefins, typically following a Schulz-Flory distribution, through a coordination-insertion chemistry (so-called *true oligomerization* mechanism) analogous to that reported for the homogeneous catalysts. At this point, it is pertinent to mention that, even though cationic Ni species in exchange positions have been generally postulated as the active sites in this mechanism, the oxidation state of the active Ni sites still remains controversial. This issue will be analyzed in more detail in section 3.3 on the basis of CO-FTIR experiments.

The most commonly studied acid carriers in Ni-based bifunctional ethylene oligomerization catalysts are amorphous SiO_2-Al_2O_3 [3,4,12], Al-MCM-41 [5,6], and zeolites [7,8,9,10,11]. Thus, besides Ni sites, these catalysts do also typically bear Brønsted-type acidity due to protons associated to tetrahedral AlO_4^- entities whose charge was not compensated by Ni cations. Depending on their amount and strength as well as on the reaction conditions (i.e. temperature), further oligomerization of C_{4+} alkenes into larger alkenes, isomerization, hydrogen transfer, and cracking (β-scission) reactions may also take place to different extents on the Brønsted acid sites. As a result, a complex hydrocarbon mixture comprising both linear and branched as well as even and and odd numbered alkenes is produced. The acid-catalyzed route is usually referred to as *hetero-oligomerization* pathway. By properly tuning the properties of the bifunctional catalyst (Ni/H^+ ratio, number and strength of the Brønsted acid sites, porosity, etc.) and reaction conditions one should be able, *a priori*, to tailor the carbon number distribution and degree of branching of the final

product. In this way, a mixture of highly branched C_5-C_{12} alkenes could be selectively produced which, upon a simple hydrogenation step, might be marketed as a high octane gasoline component. This feature endows the heterogeneous ethylene oligomerization process using bifunctional Ni-based catalysts with a higher flexibility regarding the product slate as compared to the traditional homogeneous processes. Microporous Ni-zeolite catalysts are, in principle, well suited to this purpose given the large variety of available pore structures and the possibility to fine tune their acidic properties. However, previous studies using Ni loaded on Y [8,10] and MCM-22 [9] zeolites showed that, even initially active, the catalysts experienced a rapid deactivation with time due to heavy (mostly branched) oligomers formed on strong Brønsted acid sites that remained trapped in the micropores. Introducing mesoporosity in the zeolite should facilitate the diffusion of the bulkier oligomers and should, thus, result in an improved activity and stability during the reaction. In fact, it has been recently reported that catalysts prepared by loading Ni on the pillared MCM-36 zeolite showing both micropores (inside layers) and mesopores (in the interlayer space) deactivated at a lower rate and displayed a higher activity for ethylene oligomerization than their Ni-MCM-22 counterparts lacking the interlayer mesopores [9]. Accordingly, Ni-SiO_2-Al_2O_3 [3,4] and Ni-Al-MCM-41 [6] catalysts having a mesoporous structure (more uniform and ordered in MCM-41 materials) were found active and resistant to deactivation in the continuous oligomerization of ethylene. Nevertheless, owing to their high hydrothermal and mechanical robustness, particularly as compared to the mesostructured M41-type aluminosilicates, the development of efficient Ni-zeolite catalysts is still of

prime relevance and would probably increase the change for industrial implementation of a heterogeneous ethylene oligomerization process.

In this work, this issue has been addressed by employing a nanocrystalline Beta zeolite which displays a relatively high and somehow organized mesoporosity associated to the interparticle space. It will be shown that novel Ni-Beta catalysts with the appropriate amount of Ni can stably and efficiently convert ethylene into a mixture of highly branched liquid oligomers at mild conditions. Finally, the nature of the active Ni species in Ni-Beta catalysts will be discussed based on *in situ* CO-FTIR experiments.

2. EXPERIMENTAL SECTION

2.1. Preparation of Ni-Beta catalysts

Two series of Ni-Beta catalysts were prepared starting from a commercial H-Beta zeolite (CP811, Si/Al=12, Zeolyst International). The average crystallite size of this sample was ca. 25 nm, as determined by transmission electron microscopy (TEM, Philips CM-10 microscope, 100 keV), thus confirming its nanocrystalline character. The first series of catalysts comprised four samples with Ni loading in the range of 1.0-2.5 wt% prepared by submitting the original H-Beta sample to up to five consecutive ion exchanges with intermediate drying steps at 100ºC. The exchanges were carried out with diluted (0.04M-0.1M) aqueous solutions of $Ni(NO_3)_2$ at 70ºC for 4 hours using a liquid-to-solid ratio of 10 cm^3/g. It was seen that increasing the number of ionic exchanges from five to eight did not result in further increases in the Ni loading. After the last exchange, the samples were calcined in flowing air at 550ºC for 3 h using a

heating rate of 1ºC/min. The second series was obtained by incipient wetness impregnation of H-Beta with aqueous solutions containing the required amount of $Ni(NO_3)_2$ to produce five samples with Ni loadings in the 1.0-10.0 wt% range. The impregnated solids were dried at 100ºC and subsequently calcined at 550ºC as described before for the ion exchanged series. The ion exchanged and impregnated samples were denoted, respectively, Ni(*x*)-B-ex and Ni(*x*)-B-im, where *x* stands for the Ni content in the final catalyst as determined by chemical analysis (ICP-OES, *Vide Infra*).

2.2. Characterization techniques

The Ni content and bulk Si/Al ratio in the calcined Ni-Beta catalysts were determined by ICP-OES (Inductively Coupled Plasma-Optical Emission Spectrometry) in a Varian 715-ES spectrometer after dissolution of the solids in an acid mixture of HNO_3:HF:HCl (1:1:3 volume ratio). X-ray powder diffraction (XRD) data were acquired in a Philips X'Pert diffractometer using monochromatized CuK_α radiation. The average crystallite size of NiO nanoparticles, whenever detected, was estimated by applying the Scherrer's equation to the (220) diffraction line at $2\theta \approx 62.9º$ (*fcc* NiO, JCPDS no. 04-0835), after correction for the instrumental broadening and assuming a shape factor k= 0.9. The more intense NiO diffraction peaks at $2\theta \approx$ 37.3º and 43.3º corresponding to the (110) and (200) planes could not be used to this purpose because of significant overlapping with the diffractions associated to the zeolite Beta structure (framework type code BEA according to the International Zeolite Association, IZA).

Textural properties of the samples were derived from the respective N_2 adsorption isotherms measured at -196ºC in an ASAP-2000 equipment (Micromeritics). Specific surface areas were calculated following the Brunauer-Emmett-Teller (BET) method and the micropore volumes determined by applying the *t*-plot approach. Prior to the adsorption measurements, the samples were degassed at 400ºC and vacuum overnight.

The acidity of the parent H-Beta zeolite and Ni-Beta catalysts was investigated by FTIR spectroscopy of adsorbed pyridine in a Nicolet 710 FTIR apparatus. To this purpose, self-supported wafers of 10 mg/cm^2 were prepared and degassed at 400ºC overnight under dynamic vacuum (10^{-6} mbar). Then, $1.8 \cdot 10^3$ Pa of pyridine were admitted to the IR cell and, after equilibration at room temperature (RT), the sample was degassed at 250ºC, the spectrum recorded at RT, and the background spectrum subtracted. The amounts of Brønsted and Lewis acid sites were calculated from the integrated areas of the pyridine bands at ca. 1450 and 1545 cm^{-1}, respectively, using the extinction coefficients reported by Emeis [13].

The nature and oxidation state of surface Ni species in sample Ni(2.5)-B-ex was studied by FTIR spectroscopy of adsorbed CO. The infrared spectra of adsorbed CO were recorded at -20ºC in a Nexus 8700 FTIR spectrometer using a DTGS detector and acquiring at 4 cm^{-1} resolution. For the IR studies, the calcined Ni(2.5)-B-ex sample was pressed into self-supported wafers of ca. 10 mg/cm^2 and introduced in an IR cell allowing *in situ* treatments in controlled atmospheres and temperatures from -176ºC to 500ºC and connected to a vacuum system with gas dosing facility. Prior to the adsorption measurements the sample was pretreated in the IR cell at 300ºC for 1 h in flowing N_2 (20

cm^3/min). Afterwards, the sample was evacuated at 300ºC for 3 h under dynamic vacuum of 10^{-5} mbar, cooled down to -20ºC, and CO dosed at increasing pressures (0.1-1.0 mbar). The IR spectrum was then recorded after each dose. An additional experiment was also done as described before but using a CO adsorption temperature of 25ºC (room temperature). In a second set of experiments, the temperature in the cell after the pretreatment of the sample in N_2 at 300ºC was lowered to 120ºC (the reaction temperature applied in the ethylene oligomerization experiments) under flowing N_2. Then, the N_2 flow was stopped and a flow of pure ethylene (5 cm^3/min) was established through the cell and allowed to react with the catalyst at 120ºC and 1 bar for 4, 14, and 60 min (in independent experiments). After each reaction time the sample was evacuated at 300ºC for 1 h under vacuum of 10^{-5} mbar, cooled down to -20ºC, and CO dosed at increasing pressures (0.1-1.0 mbar). The IR spectrum after each dose was acquired. Finally, the interaction of ethylene with different surface Ni species in the N_2-pretreated Ni(2.5)-B-ex catalyst after *in situ* reaction with pure ethylene at 120ºC for 60 min was also studied by ethylene-CO co-adsorption followed by FTIR. In these experiments CO (1 mbar) was first adsorbed at -20ºC and the spectrum registered. Then, ethylene (1 mbar) was adsorbed at the same temperature and the spectrum registered again. Afterwards, the stability of the adsorbed species was investigated by submitting the sample to increasing temperatures from -20ºC to 12ºC. Subsequently, the cell was evacuated at 12ºC and 10^{-5} mbar for 30 min, the temperature lowered to -20ºC, and 1 mbar of CO adsorbed onto the sample. Then, the IR spectra were collected.

2.3. Catalytic experiments

Ethylene oligomerization was carried out in a continuous flow fixed-bed reactor at 120ºC, 35 bar total pressure, 26 bar of ethylene (Ar as balance gas), and Weight Hourly Space Velocity (WHSV) of 2.1 $g_{C2H4}/(g_{cat} \cdot h)$. Typically, the reactor was loaded with 1.0±0.1 g of catalyst with a pellet size of 0.2-0.4 mm diluted with CSi particles (0.6-0.8 mm pellet size) so as to obtain a constant bed volume of 6.5 cm^3. Prior to the catalytic experiments, the catalysts were pretreated *in situ* in flowing N_2 (50 cm^3/min) at atmospheric pressure and 300ºC for 16 h. After the catalyst pretreatment the reactor was cooled down to the reaction temperature of 120ºC under N_2 flow and the total pressure increased to 35 bar. Then, the N_2 flow was stopped and a gas mixture comprising 74 mol% ethylene and 26 mol% Ar (used as internal standard for GC analyses) was established through the reactor. The catalytic reactions typically lasted 8-10 h. During this period, liquid products formed during the reaction were condensed in two consecutive traps located at the reactor outlet, the first one heated at 150ºC and kept at the reaction pressure, and the second one at atmospheric pressure (located after the pressure control valve) and maintained at ca. 0ºC. Uncondensed reaction products were regularly analyzed *on-line* in a gas chromatograph (Bruker 450 GC) equipped with a capillary column (BR-1 FS, 50 m x 0.25 mm x 0.50 μm), two packed columns (Hayesep Q, and Molecular Sieve 13 X), and two detectors: a TCD (Thermal Conductivity Detector) and a FID (Flame Ionization Detector). The products condensed in the two traps were collected at the end of the experiments, weighted, and analyzed *off-line* in the same gas chromatograph used for the *on-line* analyses. Carbon mass

balances, averaged through the whole experiment by combining the *on-line* and *off-line* GC analyses, fell within the 100±5% range.

The conversion of ethylene at a given time-on-stream (TOS) was calculated from the relative areas of ethylene and Ar (internal standard) at the reactor inlet and outlet obtained in the TCD *on-line* analysis and considering the respective response factors. The carbon number distribution of the oligomers formed (in wt%) was averaged for the whole experiment by combining the results of the *on-line* and *off-line* analyses.

In order to quantify the degree of branching in certain carbon fractions (C_6-C_8), the liquids condensed in the two traps were mixed and fully hydrogenated in a batch reactor so as to produce a mixture of alkanes which allows for an easier identification of the linear and branched isomers by GC. Typically, about 0.5 cm^3 of the liquid oligomerization product were hydrogenated at 70ºC, and 30 bar using ca. 200 mg of a commercial Pd catalyst supported on activated charcoal (10 wt% Pd, Fluka) previously reduced in flowing H_2 at 180ºC for 3 h. The hydrogenated product was then analyzed in the same gas chromatograph used in the oligomerization reaction. Identification of alkane isomers in selected carbon fractions was done by comparing the retention times with those of commercially available standard hydrocarbon mixtures.

3. RESULTS AND DISCUSSION

3.1. Characterization of the catalysts

As expected, the bulk atomic Si/Al ratio in the Ni-Beta catalysts determined by ICP-OES matched that of the starting zeolite (Si/Al=12). The main physicochemical properties of the parent H-Beta zeolite and Ni-Beta catalysts

are presented in Table 1. The Ni content (from ICP-OES) in the ion exchanged Ni(*x*)-B-ex series varied from 1.0 to 2.5 wt% when increasing the number of ionic exchanges from 1 to 5. As intended, the impregnated catalysts contained Ni in amounts ranging from 1.1 to 10.0 wt%. In turn, Ni-Beta catalysts prepared by ionic exchange displayed values for the BET surface area (ca. 600-610 m^2/g) and micropore volume (0.19 cm^3/g) similar to those of the starting H-Beta, suggesting a high dispersion of the Ni species. By contrast, a decrease in both BET area and micropore volume was noticed for the impregnated Ni(*x*)-B-im series. In general, both parameters showed a decreasing trend with increasing Ni loading from 1.1 to 10.0 wt%. This decrease in textural parameters cannot be ascribed to a certain damage of the zeolite structure. Indeed, the crystallinity of the calcined samples relative to that of the original H-Beta (calculated from the area of the most intense BEA X-ray diffraction peak at 2θ= 22.5º) remained higher than 96% even for the highly-loaded catalysts. Therefore, it is likely due to both a “dilution effect” and a partial pore blockage caused by NiO crystallites which, as will be shown below, are readily detected by XRD in the impregnated series at Ni contents $\geq$ 3.8 wt%.

The X-ray diffractograms for the calcined ion-exchanged and impregnated catalysts are shown in Fig. 1a and 1b, respectively. For comparison purposes, the XRD of the parent H-Beta sample is also included. The high crystallinity of the zeolite in both Ni(*x*)-B-ex and Ni(*x*)-B-im samples becomes evident by comparing their diffraction patterns with that of the parent zeolite. As seen in Fig. 1a, the Ni-Beta catalysts prepared by ionic exchange did only display the diffractions corresponding to the crystalline BEA structure, further supporting a high dispersion of the Ni species in the zeolite matrix. By contrast, diffraction

peaks at ca. 37.2º, 43.3º, and 62.9º (2θ) corresponding to the (111), (200), and (220) planes of the *fcc* phase of NiO crystallites (JCPDS no. 04-0835) are apparent in the impregnated catalysts with Ni loading ≥ 3.8 wt% (Fig. 1b). The estimated average size of the NiO crystallites was about 7, 11, and 16 nm (see Experimental section for details on the calculation) for the catalysts with Ni loadings of 5.0, 5.8, and 10.0 wt%, respectively. It is obvious that such NiO nanoparticles have to be located on the external surface of the zeolite crystallites and may, thus, contribute to the larger relative decrease in BET surface area observed for these samples, as discussed before (Table 1). It should be noted that, even for catalysts with Ni loadings below 3.8 wt%, the presence of very small (< 3 nm) XRD-silent NiO nanoparticles cannot be discarded at this point.

The concentrations of Brønsted and Lewis acid sites in the parent H-Beta and Ni-Beta catalysts, as determined by FTIR-pyridine at a desorption temperature of 250ºC, are compared in Table 1. Expectedly, the amount of Brønsted acid sites (BAS) for the Ni-Beta catalysts was systematically lower (45-120 μmol/g) than for the starting H-Beta sample (160 μmol/g) regardless the Ni incorporation method used. In turn, the density of BAS decreased with increasing the Ni content for both the ion-exchanged and impregnated series. In principle, the loss in Brønsted acidity should be mostly ascribed to the exchange of protons in bridged-type Si-OH-Al groups in the zeolite framework by Ni^{2+} cations. In order to better discuss the influence of the Ni loading and the method of Ni incorporation on the Brønsted acidity of the Ni-Beta catalysts, the difference in the amount of BAS between the bare H-Beta zeolite and the calcined Ni-Beta catalysts (ΔBAS) has been plotted against the Ni content in

Fig. 2. It can be seen that, in the range of 0-2.7 wt% Ni (including both series), the amount of BAS lost increases linearly (correlation coefficient of R^2= 0.985) with the Ni loading. This fact strongly suggests that in this range of Ni contents most of the Ni should be occupying cationic exchange positions in the zeolite lattice irrespective of whether the Ni was introduced *via* ionic exchange or impregnation. By contrast, for Ni contents above 2.7 wt% (in this case only the impregnated samples are concerned), the loss in the amount of BAS increases only slightly and reaches a plateau at Ni loadings $\geq$ 5 wt%. At this point, it is worth recalling that relatively large NiO particles were clearly detected by XRD in the impregnated Ni-Beta catalysts for Ni contents $\geq$ 3.8 wt%. It seems, then, that the amount of isolated cationic Ni species occupying exchange positions in the Ni-Beta samples continuously increases with the Ni content until a "saturation" value is attained at ca. 5 wt% Ni, beyond which further incorporation of Ni exclusively results in the formation of NiO nanoparticles.

As seen in Table 1, the parent H-Beta zeolite possessed a significant amount of Lewis-type acid sites (128 μmol/g) associated to the presence of highly dispersed extraframework Al species, as confirmed by the presence of a resonance at ca. -2 ppm in its ^{27}Al MAS NMR spectrum (not shown). An increasing trend in the amount of Lewis acid sites (LAS) with increasing the Ni content in the exchanged catalysts was evidenced, reaching a value of 179 μmol/g for the Ni(2.5)-B-ex sample (Table 1). For the impregnated series, covering a broader range of metal contents, the density of LAS first increased, attained a maximum of 185 μmol/g at 3.8 wt% Ni, and then decreased with the further increase in Ni loading. The increased Lewis acidity of the Ni-Beta catalysts with respect to the parent zeolite is indicative of the creation of

additional sites of this type able to coordinate with pyridine at the studied desorpion temperature (250ºC). As deduced from the ^{27}Al MAS NMR characterization results of Ni-Beta catalysts (not shown), such new Lewis-type acid sites cannot be related to additional dealumination of the zeolite framework upon the incorporation of Ni species and calcination. Instead, as illustrated in Fig. 3 for representative samples, the infrared spectra in the pyridine region of the Ni-Beta samples clearly revealed, besides the characteristic Lewis acid band at ca. 1622 cm^{-1} related to pyridine coordinated to Al^{3+} species, the presence of a band at ca. 1610 cm^{-1} attributed to pyridine coordinatively bonded to Ni^{2+} cations [14,15]. As evidenced in Fig. 3, the latter band was absent in the original H-Beta zeolite. It can be, thus, suggested that the additional Lewis acid sites detected by pyridine in the Ni-Beta catalysts are likely related to accessible Ni^{2+} cations. Even though at Ni loadings below 3 wt% these Ni-related LAS could be mostly associated to isolated Ni^{2+} species in ion exchange positions, as previously discussed, a certain contribution to the “extra” Lewis acidity of coordinatively unsaturated Ni^{2+} sites on the surface of small NiO crystallites cannot be disregarded.

3.2. Ethylene oligomerization experiments

As discussed in the Introduction section, a rapid deactivation during the oligomerization of ethylene has been previously reported for microporous Ni-zeolite catalysts [8,9,10]. Conversely, under the applied reaction conditions (T= 120ºC, P_{tot}= 35 bar, P_{C2H4}= 26 bar, WHSV= 2.1 h^{-1}) none of the Ni-Beta catalysts prepared in the present work showed apparent signs of deactivation within the studied range of TOS (0-9 h), as exemplified in Fig. 4 for selected

samples covering the full range of compositions. It is evident in Fig. 4 that, depending on the particular Ni-Beta catalyst, the ethylene conversion varied in the interval of 5-90% (samples not included in Fig. 4 displayed intermediate conversions). The influence of Ni content on ethylene conversion for the two series of Ni-Beta catalysts is presented in Fig. 5. It is seen there that for both series the conversion increased almost linearly with increasing the Ni loading up to ca. 2.7 wt% and, then, leveled off attaining a nearly constant value of ca. 85-87% at Ni loadings $\geq$ 5 wt%. It is remarkable that the shape of the conversion-%Ni curve practically matches that discussed before for the variation of ΔBAS with the Ni content (Fig. 2) and which was qualitatively related to the amount of isolated Ni^{2+} cations occupying ion exchange sites in the calcined catalysts. Therefore, it is quite reasonable to presume, in view of these results, that those Ni species would be the main Ni active sites responsible for the activation and oligomerization of ethylene through the mentioned *true oligomerization* pathway. The fact that the activity of the Ni-Beta catalysts is governed by the amount of active Ni sites further supports the unlikely activation of ethylene on the zeolite BAS. In the following section we will go further inside into the nature of the active Ni species by employing CO-FTIR experimentation.

As discussed in the Introduction, the residual Brønsted acidity in the bifunctional Ni-containing catalysts does also play a role in determining the nature and carbon distribution of the formed oligomers through the so-called *hetero-oligomerizarion* route. Under the studied conditions, the Ni-Beta catalysts yielded oligomers with carbon numbers ranging from 4 to up to 16. The carbon number distribution of the oligomers formed on the different Ni-Beta catalysts, averaged from the *on-line* and *off-line* GC analyses in the whole

reaction period, is shown in Tables 2 and 3 for the ion exchanged and selected impregnated samples, respectively. For both series, catalysts with Ni loading ≤ 2.0 wt% predominantly produced butenes with a selectivity of around 70 wt%. Moreover, at the lowest Ni content (ca. 1 wt%), i.e. samples Ni(1.0)-B-ex and Ni(1.1)-B-im, propylene was also formed with a selectivity of 6-7 wt%. The propylene selectivity decreased with increasing Ni loading and became very low (< 0.2 wt%) at Ni contents ≥2.0 wt% in both the ion exchanged and impregnated catalysts. The formation of propylene can be accounted for by considering the cracking of hexenes (second major products after butenes at low conversions, *vide infra*) favored by a relatively high concentration of BAS in Ni-Beta with low Ni content (Table 1). Furthermore, it is worthy to note that for low Ni loaded samples no products higher than C_{10} were formed and that the carbon number distribution of the oligomers with even carbon atoms closely resembled that expected for the statistical Schulz-Flory-type distribution ($C_4 > C_6 > C_8 > C_{10}$). Both the high selectivity to butenes and the Schulz-Flory-type distribution point towards a predominance of the Ni-catalyzed *true* oligomerization pathway in the low Ni loaded Ni-Beta catalysts. Contrarily, Ni-Beta catalysts with higher Ni contents (≥ 2 wt%) produced significant amount of higher oligomers, of up to 16 carbon atoms, following a non-Schulz-Flory distribution (for the sake of clarity the oligomers with 13 to 16 carbon atoms have been grouped as C_{13+} in Tables 2 and 3). These facts clearly indicate the occurrence of further oligomerization events on the remaining zeolite BAS (*hetero-ologomerization* route). As also seen in Tables 2 and 3, odd-carbon numbered products were also formed in all catalysts though with a much lower selectivity (representing, for instance, less than 4 wt% of the C_4-C_{12} fraction). The presence of odd-carbon products is

suggestive of the occurrence of secondary cracking reactions. Note that this is necessarily the case for C_5 alkenes, whereas larger odd-carbon products may also form by co-dimerization of C_{4+} alkenes on the zeolite BAS since, in this case, no primary carbocations will be involved.

In principle, it would be expected that the higher the amount of butenes formed (that is, the higher the conversion of ethylene) on the Ni sites, the higher the extent of the contribution of the acid-catalyzed oligomerization to the formation of larger alkenes would be. In other words, the distribution of the formed oligomers would expectedly be dependent on the ethylene conversion. Since the Ni-Beta catalysts were seen to display different ethylene conversions depending on the Ni loading (Figs. 4 and 5), it would be interesting to study whether or not the observed carbon distribution of the formed oligomers is exclusively a function of the conversion. To this respect, the selectivity to the predominant even carbon-numbered oligomers (taking the alkenes with 13 or more carbon atoms as a single fraction, C_{13+}) has been plotted against the conversion of ethylene in Fig. 6. According to the observed trends, it is apparent that the distribution of the oligomer products obtained on Ni-Beta catalysts is primarily a function of the ethylene conversion. Moreover, by extrapolating the selectivity curves at zero conversion it is inferred that butenes, hexenes, octenes, and decenes are apparent primary products whereas dodecenes and larger alkenes are clearly secondary. At low conversions, the (apparent) primary products are obviously formed on the Ni sites while, at higher conversions, secondary products are likely produced from the primary ones *via* acid catalysis on the zeolite BAS. It is also evident from Fig. 6 that butenes and hexenes are unstable products, indicating that they are consumed on the zeolite acid sites to

produce larger alkenes. Indeed, a net formation of octenes and decenes *via* acid-catalyzed dimerization of lower alkenes at increasing ethylene conversions is perceived in Fig. 6.

Apart from increasing the average chain length of the oligomers, as seen before, the *hetero-oligomerization* route occurring on the zeolite BAS also lead to the formation of branched products. The degrees of branching (given as iso/(iso+n) ratios) for C_6, C_8, and C_{10} oligomers as well as the distributions of C_8 isomers are given in Table 4 for selected ion exchanged and impregnated catalysts. As seen there, similar degrees of branching were found for the different Ni-Beta catalysts. The iso/(iso+n) ratios for the C_6, C_8, and C_{10} fractions amounted to 0.17-0.20, 0.87-0.89, and 0.97-0.98, respectively. Since as discussed before cracking of heavy oligomers appeared to occur to a relatively low extent on Ni-Beta catalysts at the studied conditions, it is reasonable to assume that the formation of branched oligomers mainly takes place by skeletal isomerization of linear oligomers *via* PCP (protonated cyclopropane) intermediates. The observed trend in iso/(iso+n) ratios for the analyzed fractions is, thus, the consequence of an increasingly favorable branching isomerization as the carbon chain length increases. As also shown in Table 4, all Ni-Beta catalysts lead to an alike distribution of C_8 isomers, with predominance of dibranched isomers (ca. 65%) followed by monobranched (ca. 20%), linear (ca. 10-13%), and tribranched, the latter representing only ca. 1% of the total C_8 products. The above results suggest that the C_8-C_{12} olefinic fraction produced in the oligomerization of ethylene on Ni-Beta catalysts could be suitably used, after a simple hydrogenation step, as a high octane gasoline blending component.

3.3. Nature of active Ni sites in Ni-Beta catalysts

As commented in the Introduction, the nature of the Ni species responsible for the activation of ethylene and its oligomerization (*true-oligomerization* pathway) in bifunctional Ni-based heterogeneous catalysts is still a matter of controversy. For instance, in a precedent work Yashima et al. [16] proposed zerovalent Ni (Ni^0) highly dispersed in the zeolite matrix as the active site. Contrarily, Wendt et al. [17] concluded that the sites responsible for ethylene dimerization in Ni-Al_2O_3/SiO_2 samples were coordinatively unsaturated isolated Ni^{2+} ions with Al^{3+} ions in the neighborhood. In line with this work, Ni^{2+} ions were also proposed in a more recent study by Tanaka et al. [18] as the active sites for ethylene dimerization in nickel ion-loaded mesoporous MCM-41 silica catalysts prepared by the "template-ion exchange" (TIE) method. However, a close inspection of the earlier literature covering different types of bifunctional Ni-based catalysts reveals that there are more opinions in favor of isolated monovalent Ni^+ cations as the active centers [12,19,20,21,22,23]. To make the problem more intricate, Lallemand et al. [24] recently proposed that both Ni^+ and dehydrated Ni^{2+} species compensating the framework charge of a mesoporous Al-MCM-41 carrier were catalytically active in the oligomerization of ethylene. The formation of Ni^+ in those studies was generally accounted for by partial reduction of isolated Ni^{2+} upon thermal activation of the catalyst at ambient or sub-ambient pressure [19,20,21,22,24], reduction with H_2 [22] or CO at high temperatures (350-450ºC), [21,25,26], or even upon contact of the catalyst with ethylene [19,20]. It is pertinent to mention here that in most of the above studies the conclusion that monovalent Ni^+ species are the active sites relied on room

temperature CO-FTIR characterization results [12,19,20,21,24]. In a few cases, Ni^{+} species were also detected by EPR spectroscopy [19,20,22]. It should be noted, however, that EPR is not able to detect Ni^{2+} ions and that in one of those works [22] the concentration of Ni^{+} ions detected by EPR was estimated to be only 1-2% of the total Ni present in the catalyst (NiCaY zeolite). Therefore, in our opinion the conclusions based on either EPR or room temperature CO-FTIR characterizations are open to question. In order to shed more light into the oxidation state of the active Ni species and to assess whether or not CO-assisted reduction of Ni^{2+} to Ni^{+} may take place at room temperature, CO-FTIR experiments at both room temperature (25ºC) and at -20ºC were performed on the Ni(2.5)-B-ex catalyst. Additionally, CO-ethylene co-adsorption FTIR experiments were also performed as detailed in section 2.2.

The CO-FTIR spectra collected at room temperature (25ºC) and at -20ºC (1 mbar CO) for the Ni(2.5)-B-ex catalyst pretreated *in situ* at 300ºC in flowing N_2 are compared in Fig. 7. At both adsorption temperatures the spectra showed IR bands at 2212 (with a shoulder at 2201 cm^{-1}) and 2150-2155 cm^{-1} which are associated to CO adsorbed on Ni^{2+} in, respectively, ion exchange positions (in different coordination environments) and in NiO species [24,25,26]. Two additional IR bands at 2138 and 2096 cm^{-1} related to $Ni^{+}(CO)_2$ complexes [24,25,26] were clearly perceived in the IR spectrum recorded at room temperature (spectrum a). Interestingly, these bands were not observed when CO was adsorbed at -20ºC (spectrum b). These results unambiguously show that adsorption of CO at room temperature induces the reduction of Ni^{2+} ions to Ni^{+} and, therefore, questions any conclusion regarding the nature of active Ni sites exclusively relying on room temperature CO-FTIR experiments. It is also

worth noting that not all the Ni species in sample Ni(2.5)-B-ex occupied ion exchange positions in the zeolite lattice but also a part existed as NiO entities. The fact that no NiO crystallites were detected in this sample by XRD (Fig. 1a) suggests that they are present in too low concentrations and/or as small-sized, XRD-silent, nanoparticles.

On the other hand, the IR spectra of CO adsorbed at -20ºC on the N_2-pretreated sample after *in situ* reaction (1 bar) with ethylene at 120ºC for selected times are presented in Fig. 8. The IR spectrum after 4 min of reaction (spectrum a) showed the bands at 2212 and 2150 cm^{-1} associated to Ni^{2+} species in ion exchange positions and in NiO nanoparticles, respectively. Interestingly, no carbonyls due to CO adsorption on monovalent Ni^{+} species were detected, even though the catalyst turned to be active from the very early stages of the reaction as inferred from the lack of an induction period. Reaction with ethylene for 14 min lead to the appearance of the dicarbonyl $Ni^{+}(CO)_2$ IR bands at 2139 and 2096 cm^{-1} (spectrum b). The intensity of the $Ni^{+}(CO)_2$ bands increased with the further increase in reaction time from 14 to 60 min (spectrum c). Such an increase in the intensity of the Ni^{+} carbonyls with time was, however, not paralleled with an increase in activity during the ethylene oligomerization experiments, as previously discussed. This trend and the fact that no Ni^{+} species were detected in the early reaction stages provide experimental arguments against the assignation of Ni^{+} as the catalytically active species. Instead, Ni^{+} species, which might be considered as a “product” in the sense that they are formed by reaction of Ni^{2+} with ethylene, could be contemplated as mere spectators. Other authors did also assign Ni^{+} species the role of spectators in the dimerization of butenes on a Ni/SiO_2-Al_2O_3 catalyst [15].

Therefore, our low temperature CO-FTIR results strongly pointed towards ion-exchanged Ni^{2+} species as the true active sites.

A requisite for a surface species to act as a catalytically active site is that it should be able to interact with the reactant molecule neither in a not too weak nor a too strong mode. Taking this into account, we performed ethylene-CO co-adsorption experiments followed by FTIR with the aim of further clarifying the role of Ni^{2+} and Ni^{+} species in the oligomerization reaction. The recorded IR spectra are shown in Fig. 9. As detailed in Experimental (section 3.1), the co-adsorption experiments were carried on the Ni(2.5)-B-ex catalyst after *in situ* reaction with ethylene at 120ºC (1 bar) for 60 min. The CO-FTIR spectrum of the sample in this state after adsorption of CO (1 mbar) at -20ºC corresponds to that already given in spectrum c of Fig. 8 and which is plotted again in Fig. 9 (spectrum a) for the sake of clarity. The FTIR spectrum obtained at -20ºC in the ethylene-CO co-adsorption experiment (spectrum b) revealed a strong interaction of ethylene with Ni^{2+} cations in exchange positions, as indicated by the complete disappearance of the corresponding carbonyl bands. By contrast, the interaction of ethylene with Ni^{2+} ions in NiO and with Ni^{+} turned to be, comparatively, much weaker. The stability of ethylene adsorbed on the ion-exchanged Ni^{2+} species was studied by increasing the temperature in the IR cell from -20ºC to 12ºC. After reaching 12ºC the sample was evacuated, the temperature lowered to -20ºC, and CO (1 mbar) adsorbed again onto the sample (spectrum c in Fig. 9). As it can be inferred by comparing the intensity of the CO-Ni^{2+} bands at 2212 and 2201 cm^{-1} in spectra b and c, only a fraction of the ethylene molecules were desorbed from the ion-exchanged Ni^{2+} sites after heating the sample at 12ºC. Therefore, even if ethylene was seen to

preferentially adsorb on these sites, the adsorption was not too strong so as to completely block them preventing any further adsorption of ethylene molecules.

In conclusion, the above FTIR studies provide further experimental support in favor of isolated Ni^{2+} species occupying ion exchange positions in the zeolite lattice as the main active sites responsible for the activation and *true* oligomerization of ethylene on Ni-Beta catalysts.

4. CONCLUSIONS

In this work we have reported new active and stable bifunctional Ni-Beta (Si/Al= 12, Ni= 1-10 wt%) catalysts for the oligomerization of ethylene under mild reaction conditions. At Ni loadings up to 2.7 wt%, nickel in Ni-Beta catalysts was mostly present as isolated cationic species occupying exchange positions in the zeolite lattice irrespective of whether the Ni was incorporated by ionic exchange or impregnation from $Ni(NO_3)_2$ solutions. Conversely, NiO nanoparticles residing on the outer zeolite surface were detected by XRD at higher Ni contents (impregnated catalysts). The activity of Ni-Beta catalysts for the oligomerization of ethylene (T= 120ºC, P_{tot}= 35 bar, $P_{ethylene}$= 26 bar, WHSV= 2.1 h^{-1}) increased linearly with increasing the Ni loading up to 2.7 wt% and then leveled off until a constant conversion of ca. 85-87% was reached at loading above 5 wt%. No signs of deactivation were observed for any catalyst under the investigated conditions. A good qualitative correlation was found between the ethylene conversion and the amount of Brønsted acid sites lost upon Ni loading (as determined by FTIR-pyridine) and, thus, with the amount of isolated Ni cations in exchange positions. Such Ni species were responsible for the initial activation of ethylene and its oligomerization to linear alkenes, mainly butenes, hexenes,

and octenes following a Schulz-Flory type distribution, through the so-called *true oligomerizarion* pathway. These alkenes then underwent double-bond and alkyl-shift isomerization, oligomerization, and cracking (to a lower extent) reactions on the zeolite Brønsted acid sites yielding a non-Schulz-Flory mixture of even (predominant) and odd C_5-C_{16} oligomers with a relatively high degree of branching (*hetero-oligomerization* route).

Due to the existing controversy in the previous literature, low temperature (-20ºC) CO adsorption and CO-ethylene co-adsorption FTIR experiments were performed in order to shed more light into the nature and oxidation state of the active Ni species. Based on the results from this FTIR study, isolated Ni^{2+} cations in exchange positions were proposed as the likely active Ni sites in Ni-Beta catalysts. Conversely, monovalent Ni^{+} species, which readily formed by reduction of Ni^{2+} upon adsorption of CO at room temperature or by reaction with ethylene at the reaction temperature, were assigned the role of spectators.

Acknowledgments

This paper reports work undertaken in the context of the project "OCMOL, Oxidative Coupling of Methane followed by Oligomerization to Liquids". OCMOL is a Large Scale Collaborative Project supported by the European Commission in the 7th Framework Programme (GA nº 228953). For further information about OCMOL see: http://www.ocmol.eu or http://www.ocmol.com. S.M. thanks ITQ for a predoctoral fellowship.

References

[1] D.S. McGuiness, Chem. Rev. 111 (2011) 2321-2341.

[2] M.O. de Souza, L.R. Rodrigues, H.O.Pastore, J.A.C. Ruiz, L. Gengembre, R.M. Gauvin, R.F. de Souza, Microp. Mesopor. Mater. 96 (2006) 109-114.

[3] J. Heveling, C.P. Nicolaides, M.S. Scurrell, Appl. Catal. A 173 (1998) 1-9.

[4] M.D. Heydenrych, C.P. Nicolaides, M.S. Scurrell, J. Catal. 197 (2001) 49-57.

[5] V. Hulea, F. Fajula, J. Catal. 225 (2004) 213-222.

[6] M. Lallemand, A. Finiels, F. Fajula, V. Hulea, Chem. Eng. J. 172 (2011) 1078-1082.

[7] L. Bonneviot, D. Olivier, M. Che, J. Mol. Catal. 21 (1983) 415-430.

[8] J. Heveling, A. Van der Beek, M. de Pender, Appl. Catal. 42 (1988) 325-336.

[9] M. Lallemand, O.A. Rusu, E. Dumitriu, A. Finiels, F. Fajula, V. Hulea, Appl. Catal. A 338 (2008) 37-43.

[10] M. Lallemand, A. Finiels, F. Fajula, V. Hulea, Appl. Catal. A 301 (2006) 196-201.

[11] F.T.T. Ng, D.C. Creaser, Appl. Catal. A 119 (1994) 327-339.

[12] J.R. Sohn, W.C. Park, S.E. Park, Catal. Lett. 81 (2002) 259-264.

[13] C.A. Emeis, J. Catal. 141 (1993) 347-354.

[14] M.I. Vázquez, A. Corma, V. Fornés, Zeolites 6 (1986) 271-274.

[15] A. Brückner, U. Bentrup, H. Zanthoff, D. Maschmeyer, J. Catal. 266 (2009) 120-128.

[16] T. Yashima, Y. Ushida, M. Ebisawa, N. Hara, J. Catal. 36 (1975) 320-326.

[17] G. Wendt, J. Finster, TR. Schöllner, H. Siegel, Stud. Surf. Sci. Catal. 7 (1981) 978-992.

[18] M. Tanaka, A. Itadani, Y. Kuroda, M. Iwamoto, J. Phys. Chem. C 116 (2012) 5664-5672.

[19] T. Cai, D. Cao, Z. Song, L. Li, Appl. Catal. A 95 (1993) L1-L7.

[20] T. Cai, Catal. Today 51 (1999) 153-160.

[21] A.A. Davydov, M. Kantcheva, M.L. Chepotko, Catal. Lett. 83 (2002) 97-108.

[22] I.V. Elev, B.N. Shelimov, V.B. Kazansky, J. Catal. 89 (1984) 470-477.

[23] M. Hartmann, A. Pöppl, L. Kevan, J. Phys. Chem. 100 (1996) 9906-9910.

[24] M. Lallemand, A. Finiels, F. Fajula, V. Hulea, J. Phys. Chem. C 113 (2009) 20360-20364.

[25] K. Hadjiivanov, H. Knözinger, M. Mihaylov, J. Phys. Chem. B 106 (2002) 2618-2624.

[26] A. Penkova, S. Dzwigaj, R. Kefirov, K. Hadjiivanov, M. Che, J. Phys. Chem. C 111 (2007) 8623-8631.

Table 1. Physicochemical properties of the parent H-Beta zeolite and Ni-Beta catalysts.

Sample	Ni content (wt%)	BET area (m^2/g)	Vmicro[a] (cm^3/g)	Acidity (μmol/g)[b]	
				BAS	LAS
H-Beta	-	608	0.190	160	128
Ni(1.0)-B-ex	1.0	602	0.187	118	108
Ni(1.7)-B-ex	1.7	601	0.186	103	141
Ni(2.0)-B-ex	2.0	610	0.189	93	170
Ni(2.5)-B-ex	2.5	600	0.186	70	179
Ni(1.1)-B-im	1.1	581	0.182	120	124
Ni(2.7)-B-im	2.7	581	0.184	65	144
Ni(3.8)-B-im	3.8	552	0.175	58	185
Ni(5.0)-B-im	5.0	551	0.176	48	163
Ni(5.8)-B-im	5.8	539	0.172	42	147
Ni(10.0)-B-im	10.0	504	0.165	45	139

[a] Volume of micropores.

[b] BAS and LAS are the amount of Brønsted acid sites and Lewis acid sites, respectively, as determined by FTIR of adsorbed pyridine at a desorption temperature of 250ºC.

Table 2. Averaged carbon number distribution of the reaction products formed in the oligomerization of ethylene on Ni-Beta catalysts prepared by ionic exchange[a].

Catalyst	Ni(1.0)-B-ex	Ni(1.7)-B-ex	Ni(2.0)-B-ex	Ni(2.5)-B-ex
Ethylene conversion (%)	7.2	26.9	39.4	74.9
Distribution (wt%):				
C_3	7.0	1.8	0.1	0.1
C_4	69.9	72.3	67.3	38.1
C_5	1.2	0.7	0.3	0.3
C_6	13.2	13.4	10.1	8.4
C_7	0.1	0.5	0.3	0.5
C_8	6.5	7.2	5.7	13.8
C_9	0.0	1.0	1.0	1.6
C_{10}	2.1	2.8	5.1	15.2
C_{11}	0.0	0.1	0.4	0.9
C_{12}	0.0	0.2	3.8	10.7
C_{13+}	0.0	0.0	5.9	10.4

[a] Reaction conditions: T= 120ºC, P_{tot}= 35 bar, P_{C2H4}= 26 bar, WHSV= 2.1 h^{-1}.

Table 3. Averaged carbon number distribution of the reaction products formed in the oligomerization of ethylene on selected Ni-Beta catalysts prepared by impregnation[a].

Catalyst	Ni(1.1)-B-im	Ni(2.7)-B-im	Ni(5.0)-B-im	Ni(10.0)-B-im
Ethylene conversion (%)	10.0	65.7	87.2	86.6
Distribution (wt%):				
C_3	6.0	0.2	0.1	0.1
C_4	72.1	47.1	34.4	37.4
C_5	0.4	0.3	0.3	0.3
C_6	13.5	11.5	8.9	10.6
C_7	0.2	0.3	0.3	0.2
C_8	5.7	10.4	13.0	12.7
C_9	0.0	1.4	1.4	0.8
C_{10}	2.1	11.5	16.0	15.2
C_{11}	0.0	0.6	0.8	0.6
C_{12}	0.0	8.3	11.9	10.0
C_{13+}	0.0	8.4	12.9	12.1

[a] Reaction conditions: T= 120ºC, P_{tot}= 35 bar, P_{C2H4}= 26 bar, WHSV= 2.1 h^{-1}.

Table 4. Degree of branching of C_6-C_{10} alkenes and distribution of C_8 isomers obtained in the oligomerization of ethylene on selected Ni-Beta catalysts[a].

Catalyst	Ni(2.5)-B-ex	Ni(2.7)-B-im	Ni(5.0)-B-im	Ni(10.0)-B-im
X_{C2H4} (%)	74.9	65.7	87.2	86.6
Iso/(iso+n) ratio:				
C_6	0.19	0.20	0.18	0.17
C_8	0.89	0.87	0.89	0.87
C_{10}	0.97	0.97	0.98	0.98
C_8 distribution (%):				
Monobranched	19.9	22.6	20.9	19.8
Dibranched	67.6	63.4	67.5	66.4
Tribranched	1.0	0.9	0.7	0.7
Linear	11.5	13.1	10.9	13.1

[a] Reaction conditions: T= 120ºC, P_{tot}= 35 bar, P_{C2H4}= 26 bar, WHSV= 2.1 h^{-1}.

Figure captions

Fig. 1. X-ray diffraction patterns for the series of Ni-Beta catalysts prepared by a) ionic exchange, and b) impregnation. The diffractogram of the parent H-Beta zeolite is also included for comparison purposes.

Fig. 2. Difference in the density of Brønsted acid sites between H-Beta and Ni-Beta catalysts (ΔBAS), as determined by FTIR-pyridine at a desorption temperature of 250ºC, as a function of Ni loading.

Fig. 3. FTIR spectra in the pyridine region for H-Beta and selected Ni-Beta samples after desorbing the base at 250ºC: a) H-Beta, b) Ni(1.0)-B-ex, c) Ni(2.5)-B-ex, d) Ni(1.1)-B-im, and e) Ni(5.0)-B-im. A band at ca. 1610 cm^{-1} of Lewis acid sites associated to pyridine coordinated to Ni^{2+} ions is clearly perceived in Ni-Beta catalysts.

Fig. 4. Evolution of the conversion of ethylene with time-on-stream (TOS) for selected Ni-Beta catalysts. Reaction conditions: T= 120ºC, P_{tot}= 35 bar, P_{C2H4}= 26 bar, WHSV= 2.1 h^{-1}.

Fig. 5. Influence of Ni loading on ethylene conversion over Ni-Beta catalysts. Reaction conditions: T= 120ºC, P_{tot}= 35 bar, P_{C2H4}= 26 bar, WHSV= 2.1 h^{-1}.

Fig. 6. Selectivity to the main oligomer fractions as a function of ethylene conversion for Ni-Beta catalysts. For convenience the oligomers with 13 and more carbon atoms have been grouped as C_{13+}. Reaction conditions: T= 120ºC, P_{tot}= 35 bar, P_{C2H4}= 26 bar, WHSV= 2.1 h^{-1}.

Fig. 7. FTIR of CO (1 mbar) adsorbed on sample Ni(2.5)-B-ex at room temperature (spectrum a) and at -20ºC (spectrum b).

Fig. 8. FTIR of CO (1 mbar) adsorbed on sample Ni(2.5)-B-ex catalyst at -20ºC after *in situ* reaction with ethylene at 120ºC (1 bar) for 4 min (spectrum a), 14 min (spectrum b), and 60 min (spectrum c).

Fig. 9. FTIR of CO-ethylene co-adsorption on Ni(2.5)-B-ex: a) 1 mbar of CO adsorbed at -20ºC after *in situ* reaction of the catalyst with ethylene at 120ºC for 60 min, b) 1 mbar ethylene and 1 mbar CO co-adorbed at -20ºC, c) 1 mbar CO adsorbed at -20ºC after evacuation at 12ºC (see Experimental for further details).

Figures

Fig. 1

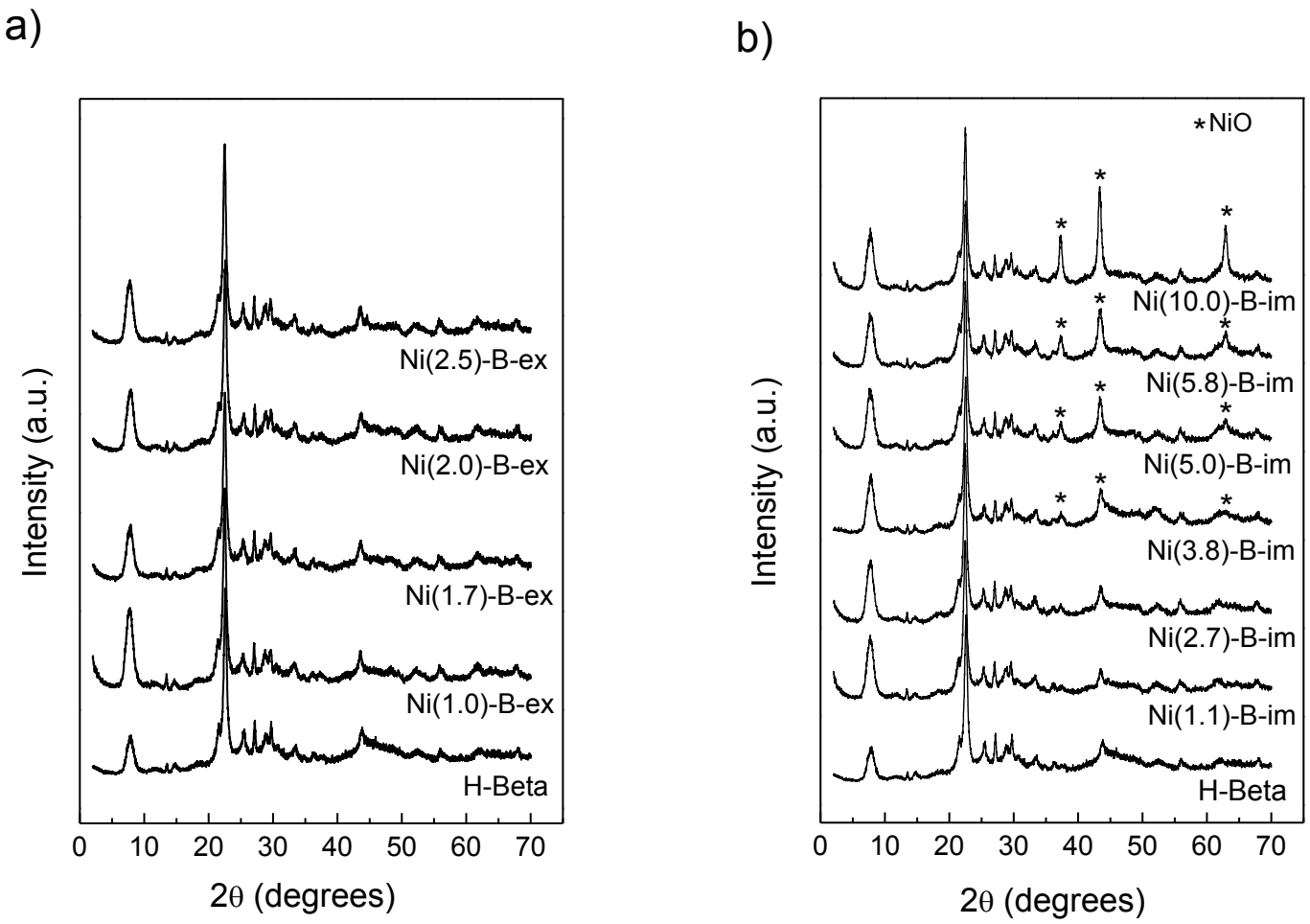

Fig. 2

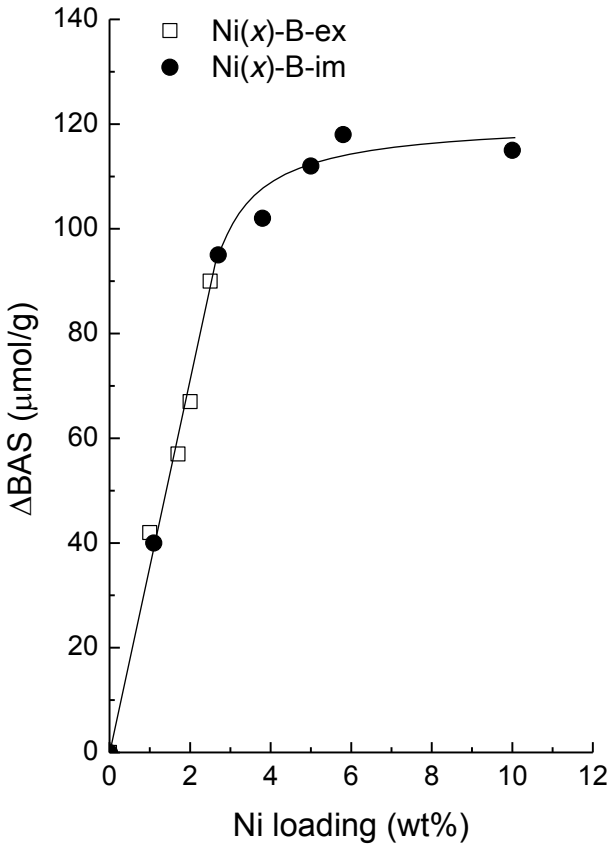
Ni(x)-B-ex
Ni(x)-B-im
ΔBAS (μmol/g)
Ni loading (wt%)
0
20
40
60
80
100
120
140
0
2
4
6
8
10
12

Fig. 3

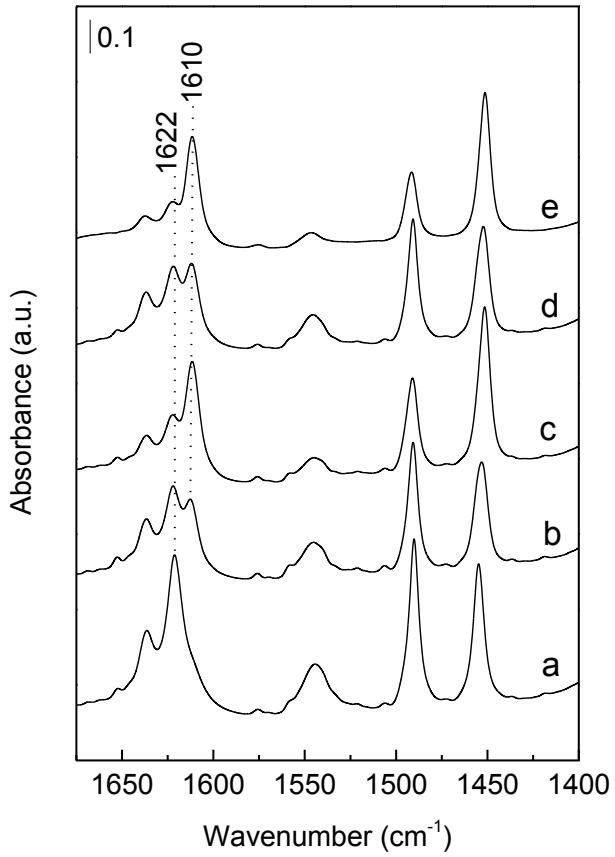
0.1
1622
1610
e
d
c
b
a
Absorbance (a.u.)
1650
1600
1550
1500
1450
1400
Wavenumber (cm-1)

Fig. 4

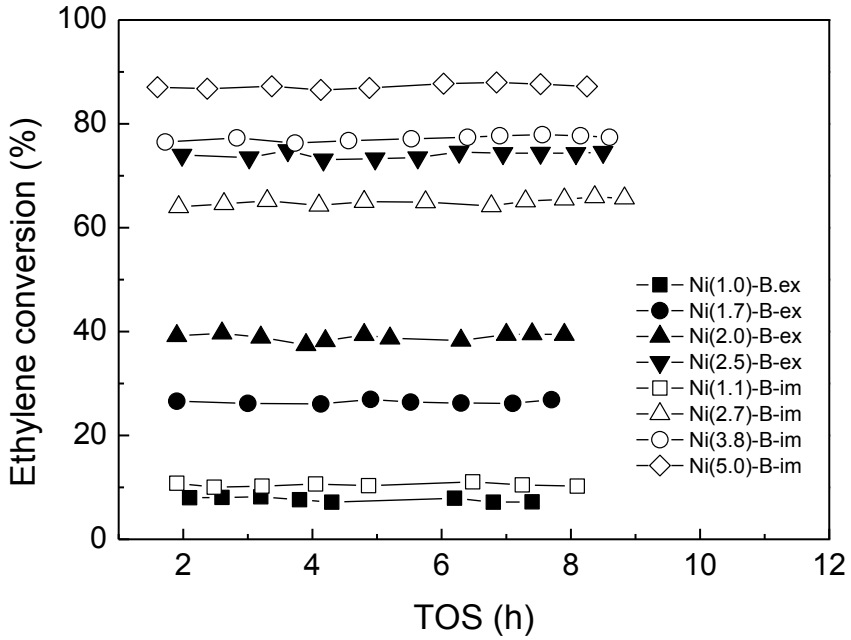
Ethylene conversion (%)
TOS (h)
0
20
40
60
80
100
2
4
6
8
10
12
Ni(1.0)-B.ex
Ni(1.7)-B-ex
Ni(2.0)-B-ex
Ni(2.5)-B-ex
Ni(1.1)-B-im
Ni(2.7)-B-im
Ni(3.8)-B-im
Ni(5.0)-B-im

Fig. 5

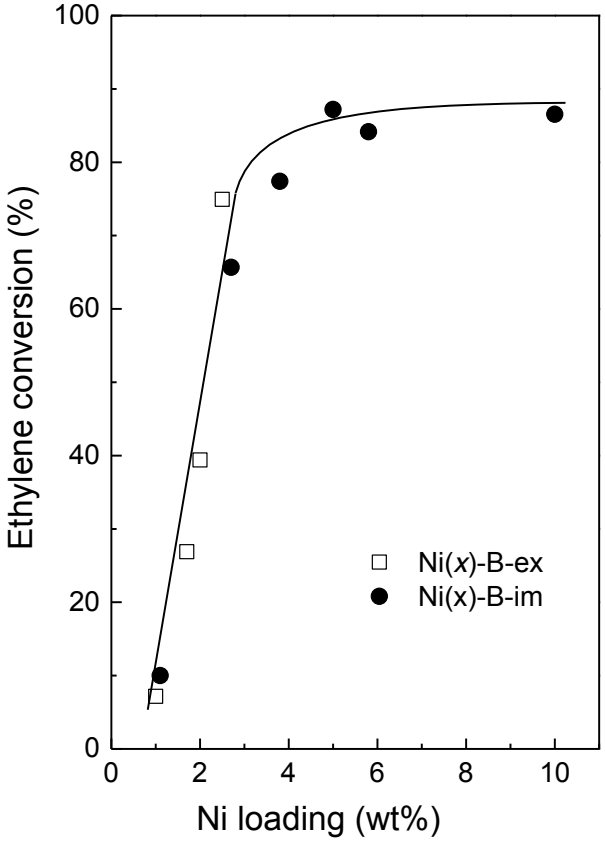
Ethylene conversion (%)
Ni loading (wt%)
Ni(x)-B-ex
Ni(x)-B-im
0
20
40
60
80
100
0
2
4
6
8
10

Fig. 6

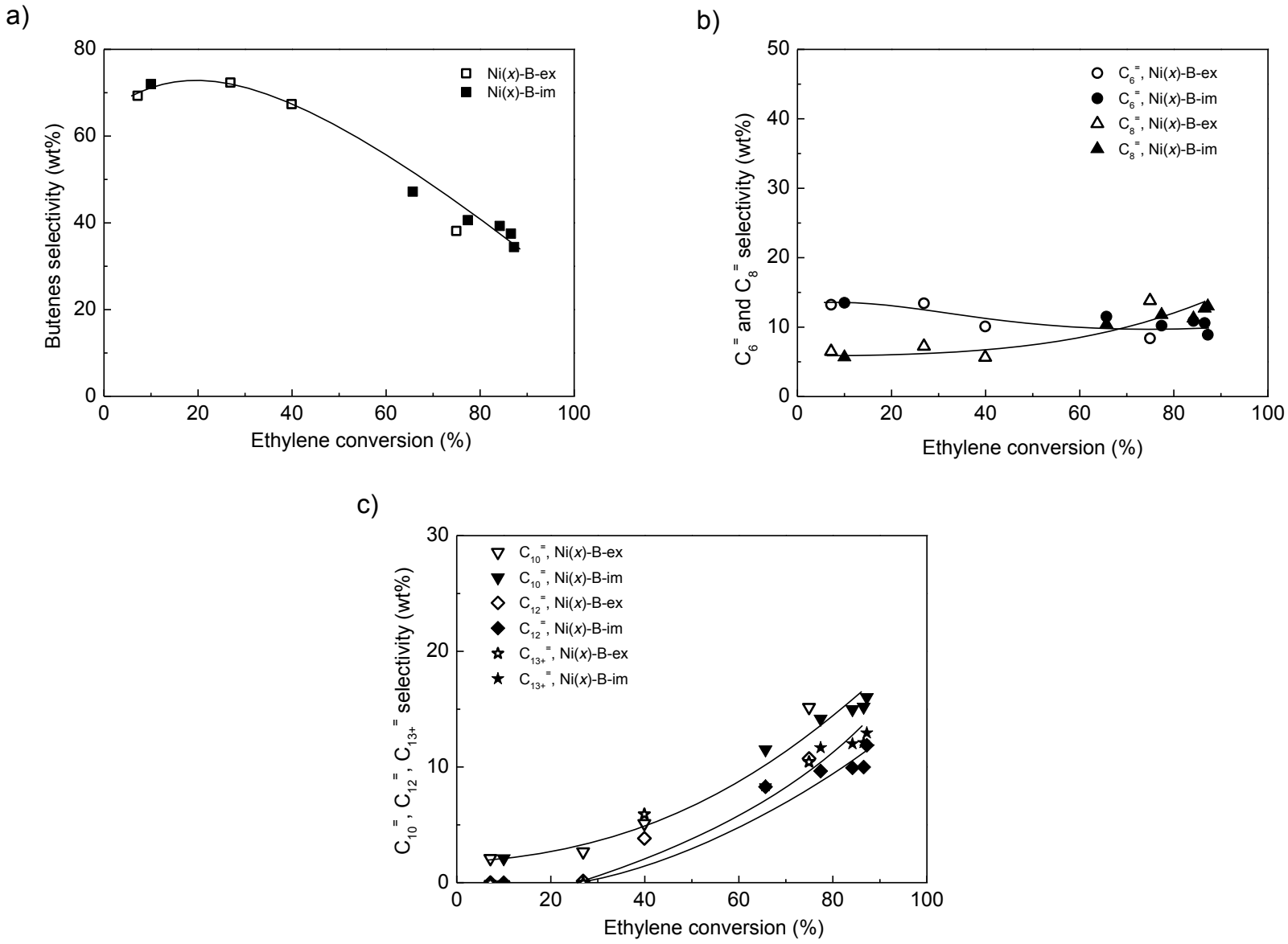
a)
Butenes selectivity (wt%)
Ethylene conversion (%)
Ni(x)-B-ex
Ni(x)-B-im
b)
C6= and C8= selectivity (wt%)
Ethylene conversion (%)
C6=, Ni(x)-B-ex
C6=, Ni(x)-B-im
C8=, Ni(x)-B-ex
C8=, Ni(x)-B-im
c)
C10= , C12= , C13+= selectivity (wt%)
Ethylene conversion (%)
C10=, Ni(x)-B-ex
C10=, Ni(x)-B-im
C12=, Ni(x)-B-ex
C12=, Ni(x)-B-im
C13+=, Ni(x)-B-ex
C13+=, Ni(x)-B-im

Fig. 7

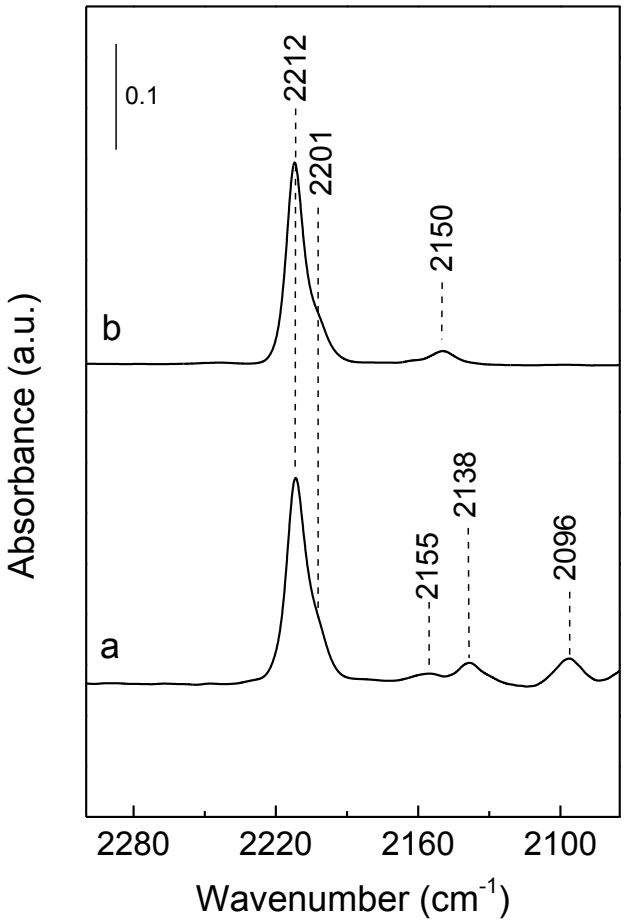
0.1
2212
2201
2150
b
2155
2138
2096
a
Absorbance (a.u.)
2280
2220
2160
2100
Wavenumber (cm-1)

Fig. 8

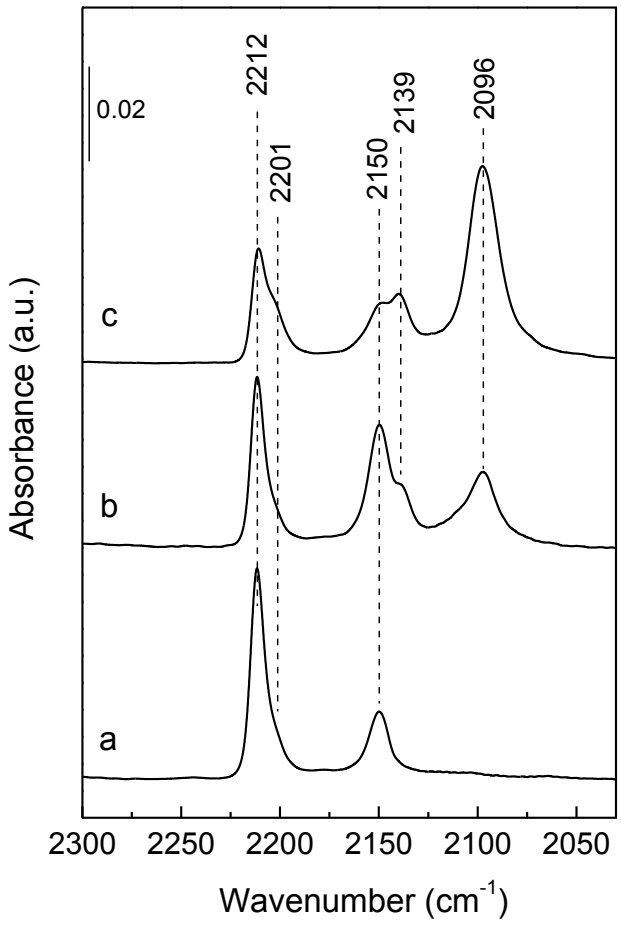
0.02
2212
2201
2150
2139
2096
c
b
a
Absorbance (a.u.)
2300
2250
2200
2150
2100
2050
Wavenumber (cm-1)

Fig. 9

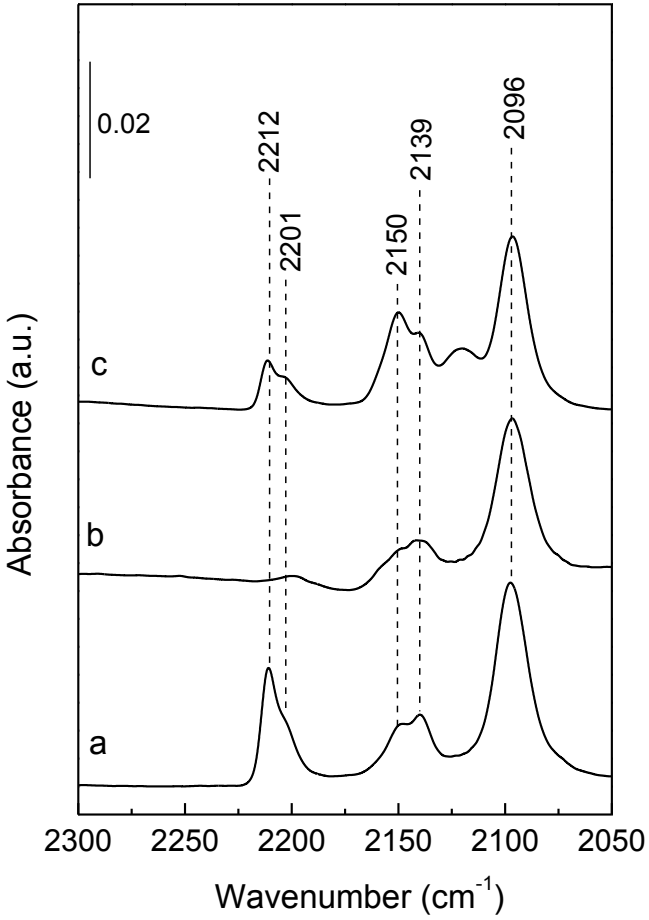
0.02
2212
2201
2150
2139
2096
c
b
a
Absorbance (a.u.)
2300
2250
2200
2150
2100
2050
Wavenumber (cm-1)

*Graphical Abstract (for review)

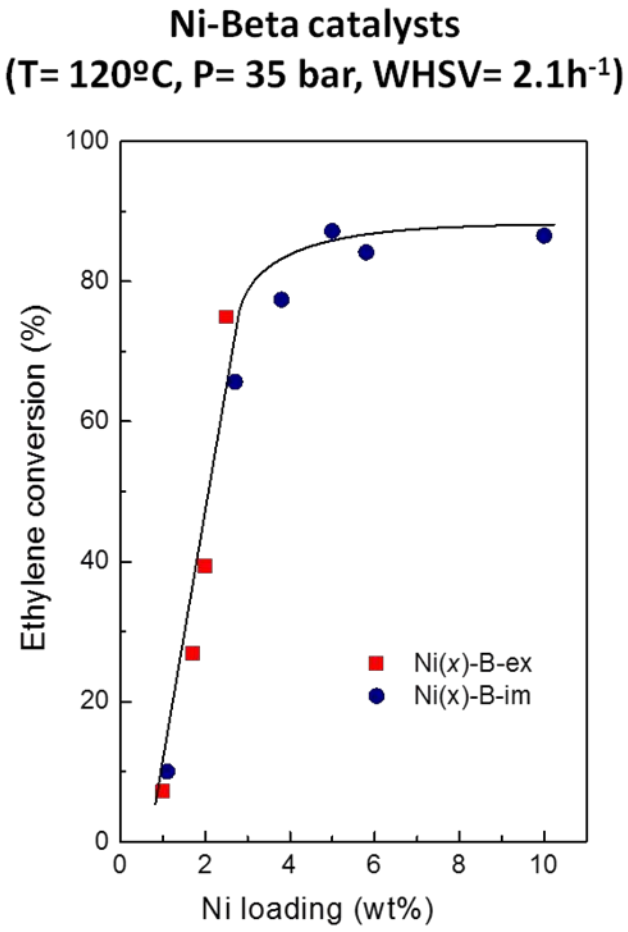

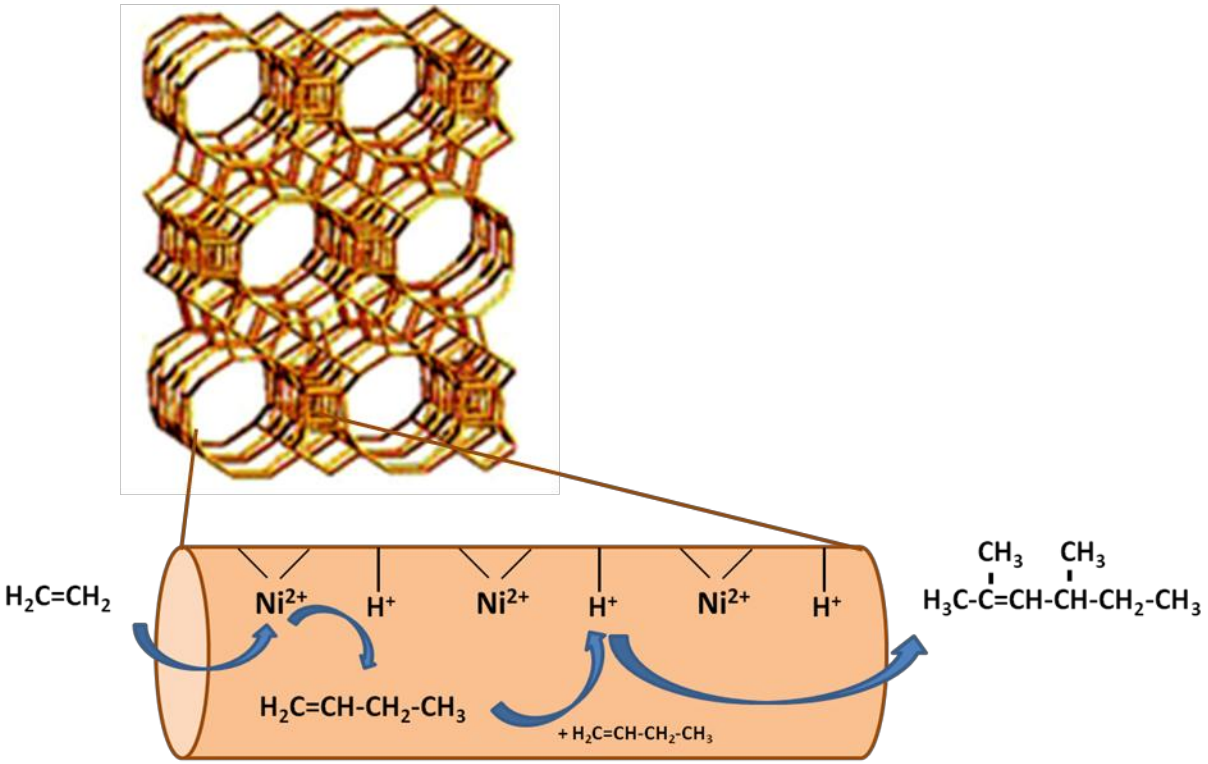

Highlights

- Bifunctional Ni-Beta catalysts are active and stable in ethylene oligomerization.
- Ni sites predominantly produce butenes and, to a lesser extent, hexenes and octenes.
- Branched C_{5+} alkenes formed by secondary oligomerization on Brønsted acid sites
- Based on CO-FTIR, Ni^{2+} cations at exchange sites are proposed as Ni active sites.